THE EUROPEAN
PHYSICAL JOURNAL C

Effect of cosmic rays irradiation on the phase change characteristics of an on-orbit fixed point

Yiru Chen[1], Caijuan Xia[1], Jian Song[2], Rui-Heng Sima[2], Jingjing Zhou[2], Yang Liu[2], Xiaofeng Tian[3], Qingxian Zhang[3], Xiaopeng Hao[2,a]

[1] College of Science, Xi'an Polytechnic University, Xi'an 710048, China
[2] Remote Sensing Calibration Laboratory, National Institute of Metrology, Beijing 100029, China
[3] College of Nuclear Technology and Automation Engineering, Chengdu University of Technology, Chengdu 610059, China

Abstract Using the phase change characteristics of fixed points to trace the temperature of a spaceborne calibration blackbody is an important technical means to carry out the high-precision on-orbit calibration of thermal infrared remote sensors. In contrast to an experimental environment on the ground, a fixed point will produce radiation damage in the high-energy cosmic rays environment and may affect the phase change characteristics. This study investigates the effect of radiation damage caused by cosmic rays irradiation on the phase change characteristics of fixed points in a spaceborne calibration blackbody. In this research, the simulation method of molecular dynamics was used to simulate the irradiation damage effect of a strong cosmic rays environment on fixed-point indium (In). The experimental system was established to measure the phase change curves of samples with different irradiation doses, and then, the influence of irradiation on the phase change characteristics of the samples was analyzed. The results showed that most of the energy of irradiation was deposited on the In fixed point, resulting in the migration of 0.3% of the displacement atoms inside the In to the gap position to form the Frenkel pairs (FPs). The overcooling of the irradiated In fixed point was reduced by 0.3 °C, the phase change temperature was increased by 30 mK, and the phase change plateau was more stable.

1 Introduction

The temperature value of a spaceborne calibration blackbody is difficult to trace on-orbit, which is the bottleneck restricting the on-orbit calibration level of thermal infrared remote sensing [1–3]. At present, a temperature sensor cannot be

[a] e-mail: haoxp@nim.ac.cn (corresponding author)

calibrated after a spaceborne calibration blackbody has been launched. Additionally, during the on-orbit operation of a spaceborne calibration blackbody, its temperature sensor is susceptible to interferences such as mechanical shock, microgravity, and space environment radiation, which lead to deviations in its temperature indication and cannot guarantee the accuracy of the value. The phase change fixed point based on the metal or nonmetal material is an important part of the International Temperature Scale (ITS-90) [4], which has the advantages of good temperature reproducibility and high accuracy. Therefore, the temperature calibration of temperature sensors using fixed points that can be embedded in a spaceborne calibration blackbody has become a research hotspot [5–8].

To achieve the practical application of phase change fixed points to an infrared remote sensing space reference blackbody source, the effect of on-orbit complex operating conditions on the phase change characteristics of fixed points needs to be considered. Widiatmo et al. [9] studied the phase change characteristics of metal Ga and analyzed the relationship between the Ga point temperature and the hydrostatic pressure of liquid Ga, the gas pressure, and the impurity content in Ga. The results showed that under non-high vacuum sealing conditions, the residual gas pressure affected the Ga point temperature and increased its uncertainty. Topham et al. [10] studied the influence of microgravity on the phase change characteristics of the fixed point. Experiments were conducted on the International Space Station with the ITS-90 standard material Ga, and it was found that within a few mK of uncertainty, no significant difference was observed between the melt temperature of the Ga at 1 g and in microgravity. Hao Xiaopeng et al. [11,12] studied the fixed point phase change plateau of Ga and Ga-In alloys and showed that the melting point temperature of the Ga and Ga-In alloy

fixed point had a good linear relationship with the heating power. Additionally, the phase-change temperature plateaus of six types of miniature fixed points, namely, H2O, Ga-Sn, Ga-Zn, PS, succinonitrile, and Ga, were tested. A linear relationship was observed between the heating power and the run-off point temperature.

In the space environment, the radiation damage effects caused by high-energy cosmic rays are also the focus of consideration. Irradiation defects are generated in the high-energy cosmic rays environment for spaceborne calibration blackbody fixed point materials, and the generation of irradiation defects can have significant effects on the mechanical and thermal properties of fixed point materials [13–15]. However, there have been few studies on the effect of cosmic rays irradiation on fixed points, and the formation process and the evolution mechanism of irradiation defects in fixed point materials are still unclear.

Due to the limitation of time and space scales, it is difficult to observe a series of processes such as the formation, migration, and aggregation of irradiation defects in a material through experiments. Molecular dynamics simulation [16] is a simulation method based on Newton's law that can study the change process of materials at the atomic scale and reveal the physical mechanism of the change of the microstructure due to irradiation. The modified embedded-atom method (MEAM) potential developed by Eun Cheol Do et al. was used for the fixed point material indium (In) [17]. The close part of the interaction potential between atoms (less than 1.0A) was docked with the Ziegler-Biersack-Littmark potential (ZBL) [18]. The Large-scale Atomic/Molecular Massively Parallel Simulator (LAMMPS) program has been successfully implanted for ZBL potential for simulating the cascade processes of irradiation collisions [19], Therefore, the simulation adopts the open-source molecular dynamics simulation program LAMMPS developed by Sandia National Laboratory in the United States.

In this research, a representative In phase change fixed point that could be applied to the thermal infrared remote sensing spaceborne temperature standard was selected. First, the In fixed point crucible was designed, and then, the energy deposition model and the molecular dynamics model of the irradiation damage of the In fixed point crucible were established. The phase change experimental test system of the In fixed point crucible irradiated by the cobalt source in a simulated space environment was built. Focusing on the basic physical problems such as the evolution of the irradiation defects and the thermodynamic mechanism of the phase change temperature plateau, the effect of space irradiation on the phase change characteristics of the fixed point for spaceborne temperature standard is discussed in this paper.
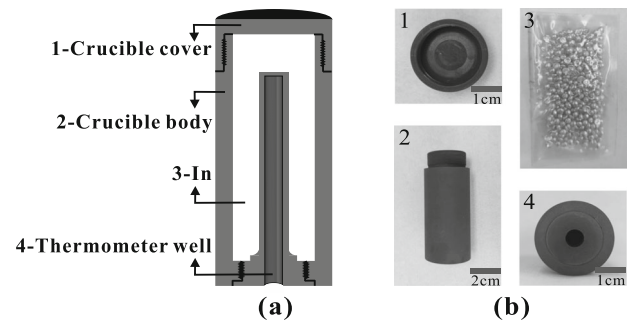

Fig. 1 **a** Design diagram of In phase change fixed point crucible; **b** 1-crucible cover; 2-crucible body; 3-metal In; 4-thermometer well

2 Model and simulation

2.1 Fixed point crucible model

To explore the effect of irradiation on the phase change characteristics of the In fixed point, the model diagram of the In fixed point graphite crucible shown in Fig. 1a was designed. Figure 1b shows the crucible physical diagram. To ensure the accurate measurement of temperature values during the phase transformation process, the thermometer well was designed at the center of the fixed point crucible. High-purity In (99.99999% purity) fixed point material was encapsulated in the crucible. The shell of the crucible was made of graphite material to ensure good thermal conductivity and high strength of the fixed point device. The shape of the entire device and the bottom was designed to be threaded to ensure good thermal conductivity. First, the effects of cosmic rays on the fixed point crucibles were simulated by energy deposition simulation in this research. Then, according to the different irradiation conditions of the fixed point crucible in the spaceborne calibration blackbody, the crucible was irradiated with six different doses (0 Gy, 99.5 Gy, 199 Gy, 298 Gy, 398 Gy, and 597 Gy) to simulate the space radiation environment.

2.2 Simulation of energy distribution of high-energy protons in a fixed point crucible

The cosmic rays that cause irradiation damage to spaceborne calibration blackbody fixed point materials are mainly high-energy protons. MCNPX (Monte Carlo N-Particle) software [20] was used to simulate the energy deposition process and distribution characteristics of high-energy protons in a fixed point crucible. Figure 2a shows the model diagram of the simulation, with graphite in the blue region and the In phase change fixed point material in the red region. The particles were high-energy protons that originate isotropically from the outer surface of the phase change fixed point crucible, and Fig. 2b shows the traces of the high-energy protons. The particle energies ranged from 0.1 to 1 GeV, and the num-
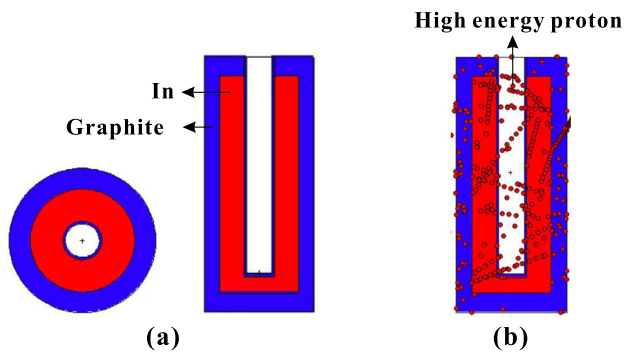
Fig. 2 Simulation model: **a** prone and orthophoto of geometric model; **b** transport diagram of particles in the model

Fig. 3 **a** Cell structure of In. **b** Supercell structure and local amplification diagram after In relaxation

ber of simulated particles was 10^9 initial particles. The dot matrix energy deposition fixed point crucible was used, and the energy deposited at each position in the fixed point crucible was recorded.

2.3 Molecular dynamics simulation of In radiation cascade

When the spaceborne temperature standard carrying the In fixed point was affected by cosmic rays, the energy of high-energy protons was mainly deposited on the fixed point material In, resulting in irradiation defects inside the In. The properties of materials were determined by the lattice dynamics caused by the change in lattice structure; that is, by the formation and migration of vacancies and interstitial clusters. In this research, the molecular dynamics simulation method was used to simulate the dynamic process of the generation and evolution of vacancies and interstitial atoms. The experimentally determined metal In had a tetragonal lattice structure that could be regarded as a face-centered tetragonal (FCT) or a body-centered tetragonal structure (BCT) [21]. Figure 3a shows a schematic diagram of the cell structure of the In at the $\langle 100 \rangle$ interface. This structure was characterized by a = b ≠ c, and it was experimentally determined that a = 3.253 Å and c = 4.947 Å. The initial model of the structure was established using the experimentally determined lattice constants, and the unit cell contained two atoms whose coordinates were (0, 0, 0) and (0.5, 0.5, 0.5).

Figure 3b shows the supercell structure of 80 × 80 × 54 used for the irradiation damage simulation of single crystal In, and a locally enlarged view of the superlattice structure, which contained 691,200 atoms and used periodic boundary conditions in four directions. The initial structure relaxed 30,000 steps (30 ps) with the constant pressure and temperature (NPT) ensemble. The set pressure and temperature were 0 Pa and 300 K, respectively. The temperature and pressure regulation methods were used in the Nose/Hoover hot bath [22] and the Nose/Hoover pressure bath [23,24], respectively. After the relaxation reached equilibrium, the lattice constants
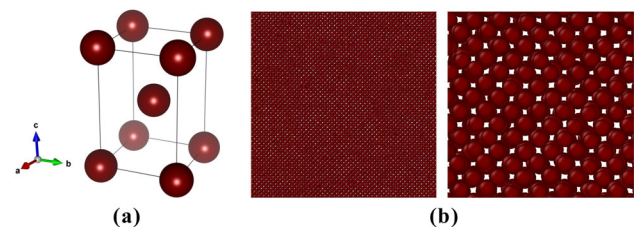
of the In were a = 3.273 Å and c = 4.969 Å, which were close to the experimental values. An arbitrary In atom near the center of the system was chosen as the primary kinetic atom (PKA) and given the kinetic energy of 10 KeV. The integral step size of PKA was in the form of variables, and the variation range was 0.01–1 fs. The four crystal directions $\langle 001 \rangle$, $\langle 100 \rangle$, $\langle 110 \rangle$, and $\langle 135 \rangle$ were selected as the outgoing directions of the PKA, and 10 trajectory simulations were performed for each outgoing direction as the result statistics, and the whole cascade collision process was carried out with the microcanonical ensemble (NVE). To eliminate the influence between the PKA and the surrounding mirror image and the excess heat in the system caused by cascade collisions, the outermost 0.3 nm of the system was set as the thermostat layer. The temperature of the thermostat layer was maintained at 300 K, and the speed of the atoms in the thermostatic layer was adjusted at consistent intervals of a specific number of steps.

3 Experimental system and process

To investigate the effect of proton irradiation on the phase change characteristics of an In fixed point crucible on-orbit, a test system for the phase change experiment of an In fixed point crucible irradiated by an electron in a simulated space environment was built, as shown in Fig. 4. To achieve stable experimental conditions for multiple repetitions, a tube furnace was specially selected to achieve the required thermal measurement environment. The experimental system mainly consisted of a tube furnace, a fixed point crucible, an insulation block, 1595 thermometer, Pt 25 platinum resistance thermometer, and inert gas. The In phase change fixed point crucible was placed at the center of the tube furnace with the same insulating material that was placed at both ends. The Pt 25 platinum resistance thermometer was coated with thermal conductive grease and placed in a thermometer well at the center of the crucible at the In phase change fixed point to ensure good thermal conductivity. The thermometer was connected with the electrical measuring instrument for the measurement of the experimental results.

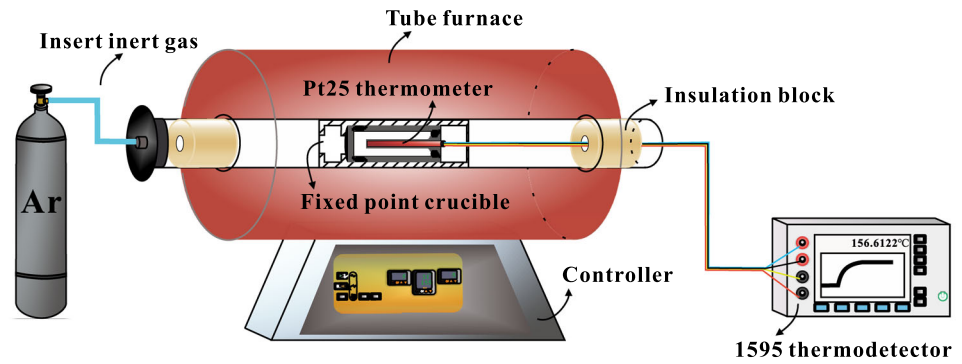Fig. 4 Experimental test system and tube furnace diagram

Table 1 Different dose conversion data

On-orbit time/year	Si-equivalent dose/Gy	In-equivalent dose/Gy	Air-equivalent dose/Gy
3	100	111	99.5
5	200	221	199
8	300	332	298
10	400	442	398
15	600	663	597

The data for the total radiation dose of 20 krad (Si) for 5 years on-orbit and 30 krad (Si) for 8 years on-orbit needed to be converted into the absorbed dose of In. At the same time, when the cobalt source was irradiated, because the radiation field was calibrated with the air absorbed dose, the absorbed dose of In needed to be converted to the air absorbed dose.

When irradiated with gamma photons, the absorbed dose under charged ion equilibrium conditions was expressed as follows:

$$D = E\varphi(\mu_{en}/\rho) \tag{1}$$

where D is the absorbed dose, in units of Gy; E is the gamma ray energy, and for Co-60 source irradiation, the average energy of 1.25 MeV is taken; φ is the Gamma photon injection; and (μ_{en}/ρ) is the mass-energy absorption coefficient of photons with energy E in the specified medium, unit cm^2/g. Therefore, the difference in absorbed doses of Si, In and air at the same photon injection under cobalt source irradiation is the difference in μ_{en}. (μ_{en}/ρ) using data provided by National Institute of Standards and Technology (NIST) was as follows: for Si: 2.652×10^{-2}, for In: 2.398×10^{-2}, and for air: 2.666×10^{-2}. Table 1 shows the conversion data for the three doses, and in the following, the samples were distinguished by the absorbed dose in air identified at the time of irradiation when the samples were analyzed after irradiation.

To simulate the effect of cosmic rays irradiation on the phase change characteristics of the fixed point graphite crucible during 15 years of on-orbit operation, six doses (0 Gy, 99.5 Gy, 199 Gy, 298 Gy, 398 Gy, and 597 Gy) were selected

to irradiate the In fixed point graphite crucible. Then, the phase change experiments were performed with six different irradiation doses for the In fixed point crucibles placed in the same thermal environment to obtain the measurements of the thermometer at the center of the crucible and to study the change in six different irradiation doses for the In fixed point performance in the same thermal environment. The experiment used a tube furnace to ensure that the insulation block and crucible were heated from the same temperature to a temperature slightly lower than the fixed point melting, and then, the same upper limit temperature was set to heat tube furnace. The upper limit temperature was the appropriate value set with the premise of ensuring the melting of the fixed point. After the tube furnace was heated, it is recommended to wait for a while. The lower limit temperature was set to solidify the fixed point material.

The specific experimental steps were as follows. First, the tube furnace was heated from room temperature to 155 °C, and the temperature began to rise after the temperature of the fixed point crucible was stable. Second, the temperature was set to 157 °C, and the heating rate was set to 0.3 °C/min in order to observe the obvious phase change platform. Third, when the In fixed point was melted and the whole system reached a thermal equilibrium state, the temperature of the furnace body was reduced to 155 °C, the cooling rate was consistent with the heating rate, and the temperature change of the sample was observed. When the In fixed point phase change was completed and the temperature was the same as the ambient temperature, the second experiment could be started. Each time, the sample was observed four consecutive times to measure the phase change process.

4 Results and analysis

4.1 Energy distribution and cascaded collision simulation analysis

First, for the spaceborne temperature standard carrying the In fixed point, using the proton irradiation accelerator, the simulation calculation results of the energy deposition and
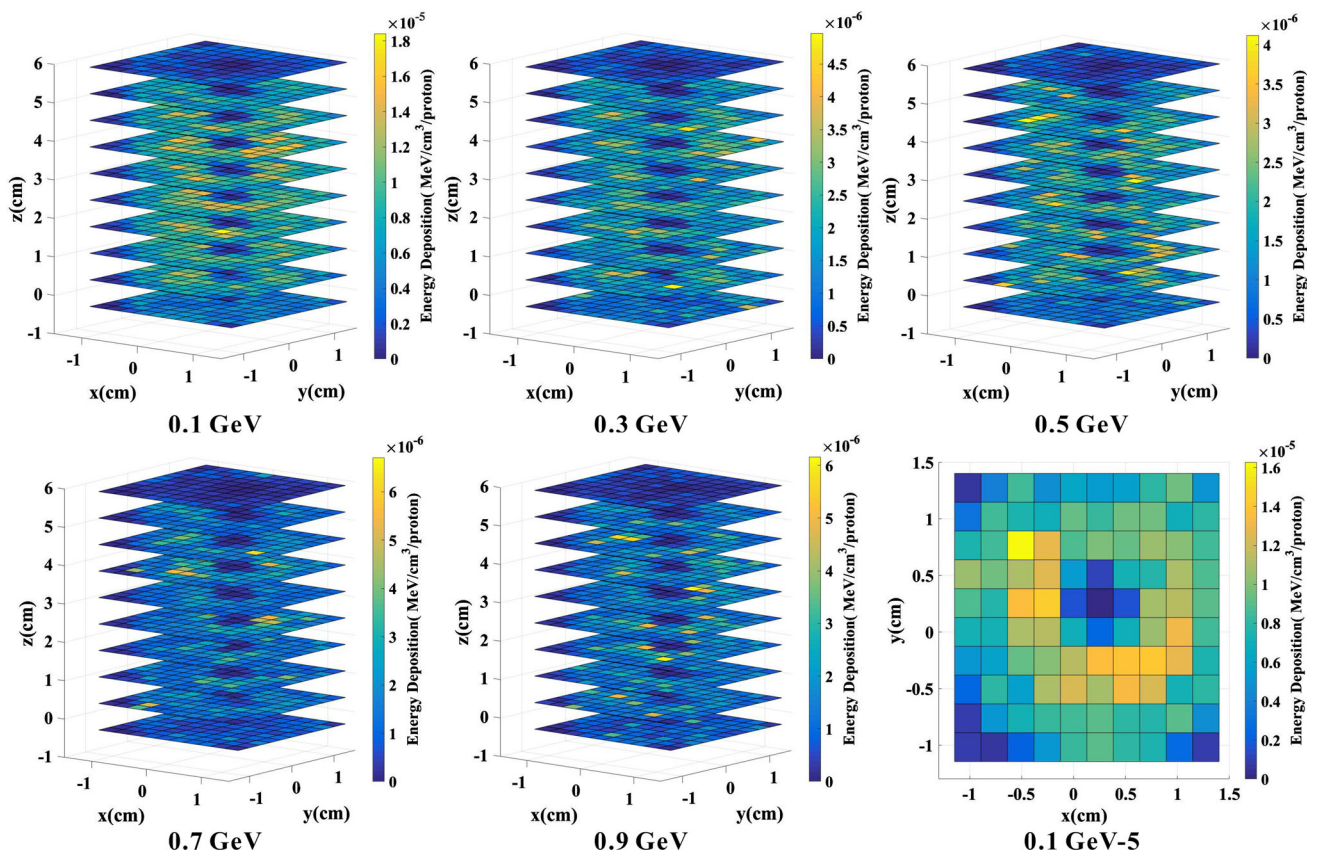
Fig. 5 Energy deposition diagram and local detail diagram at different positions

the distribution characteristics of the high-energy protons in the temperature standard were obtained, as shown in Fig. 5. The simulation calculation showed that the energy deposition on the In was relatively high, and the energy deposition on the graphite was relatively low. The magnitude of the energy deposition was related to the way in which energy was lost in the interaction between protons and matter. Since the electromagnetic interaction mainly occurred between protons and matter and the magnitude of energy deposition was proportional to the atomic number of the medium, the In materials were capable of depositing more energy. The 0.1 GeV-5 in Fig. 5 represents the detailed energy distribution of the high-energy protons at the fifth layer of the In fixed point crucible.

After the spaceborne temperature standard with the In fixed point was affected by cosmic rays, the energy of the high-energy protons was mainly deposited on the fixed point material In, resulting in irradiation defects inside the In. Afterward, the dynamic process of the generation and evolution of the irradiation defects was simulated. In the molecular dynamics simulation of the irradiation cascade collision process of the In, the Wigner–Seitz (W–S) cell method [25] was used for defect analysis. The atoms that moved away from the original lattice position by more than 1 Å due to the collision were called displaced atoms. The atoms that

moved away from the original lattice position by less than 1 Å were considered to still vibrate around the lattice. The partially displaced atoms reached the lattice sites of the other atoms, which were called replacement atoms. The displacement atoms without the formation of replacement atoms had to migrate to the gap position, forming a gap-vacancy defect pair, which was an FP.

Figure 6 shows the evolution of the FP distribution with time in the ⟨001⟩ direction of the PKA. In the figure, green represents vacancies, and red represents gaps. At t = 0, the PKA started to shoot out, after which it underwent several collisions and migrated for a long distance. In the simulations of this research, the peak phase of the collision persisted up to about 4.17 ps, and the number of defective atoms between 0 and 4.17 ps was constantly increasing. At 4.17 ps, the defective atoms at the end of the collision peak phase were shown, and then, the system entered the thermal peak phase. The excessive heat in the system due to the cascade collision started to dissipate gradually, and this process continued until about 50 ps. Then, the temperature of the system gradually decreased. After 55 ps, the number of defective atoms and their configuration no longer changed, and the system entered a stable state. This evolutionary trend is illustrated in Fig. 7. This was very similar to the initial structure of irra-

Fig. 6 Typical evolution of FP distribution with time in the ⟨001⟩ direction of the PKA

0.19ps   1.77ps   4.17ps
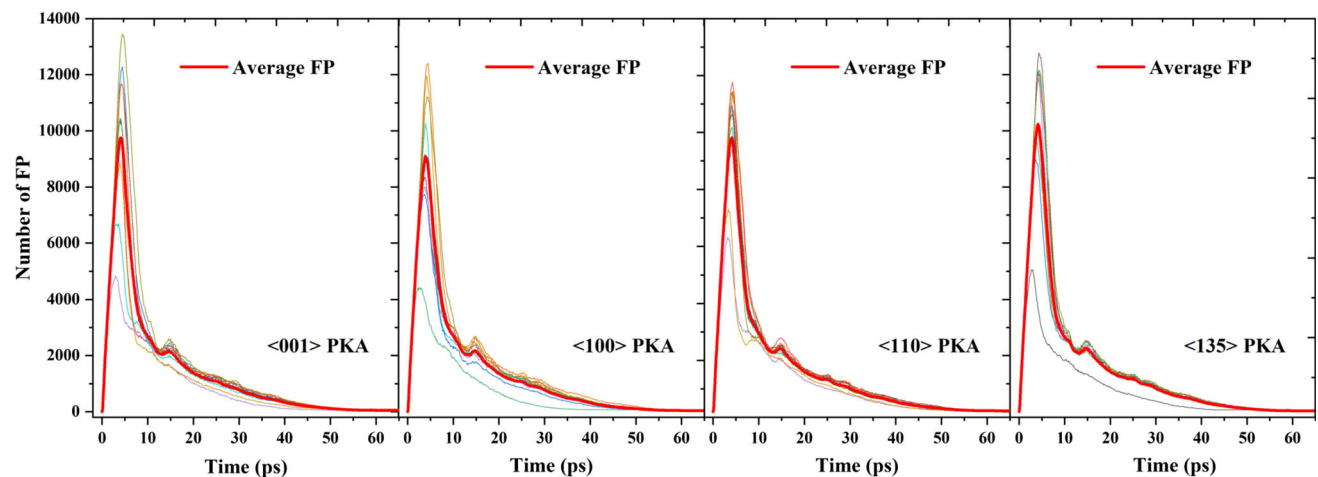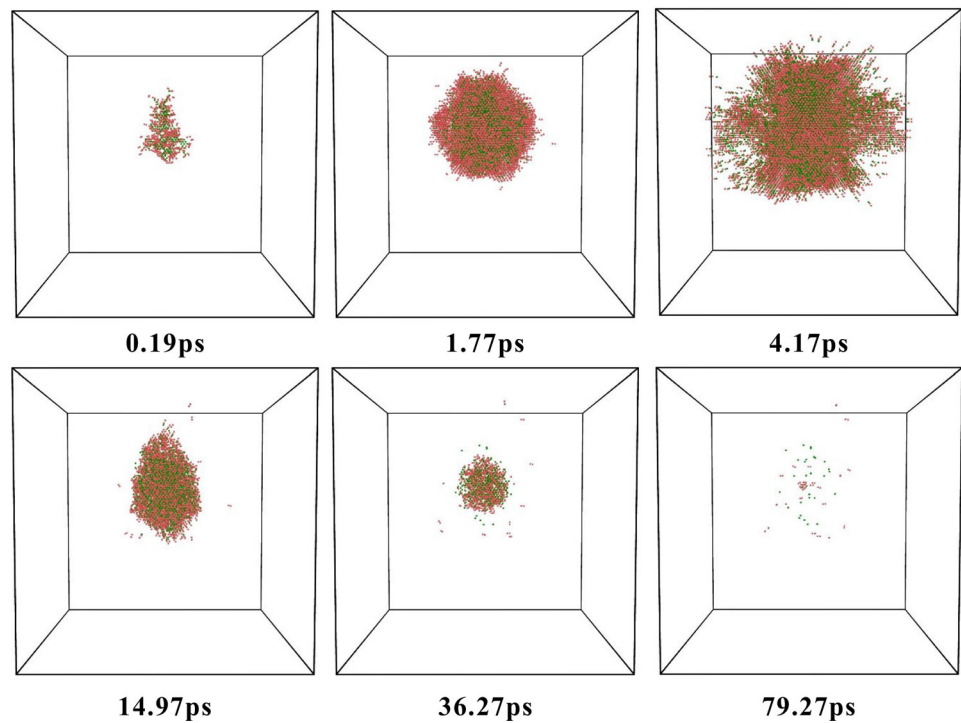
14.97ps   36.27ps   79.27ps

Fig. 7 Evolution of the FP number with time during the PKA cascade collision of the 10 keV kinetic energy in the metal In

diation cascades in crystal structures with high symmetry, and the defective atoms had recovery behavior, resulting in a decrease in the number of defective atoms [26–28].

Figure 7 shows the evolution of the FP number over time during the cascade collisions of the PKA with the kinetic energy of 10 keV and four outgoing directions of ⟨001⟩, ⟨100⟩, ⟨110⟩, and ⟨135⟩ in the metal In. The number of FPs in the four PKA directions reached a peak at about 4 ps, and the average peaks were 9746, 9075, 9752, and 9561. After 55 ps, the number of defects tended to be balanced, and the average FP numbers after balance were 47, 42, and 33. The number of defects in the ⟨100⟩ direction with the PKA was slightly lower, which was due to a statistical error. It can be

seen from the four average curves that the outgoing direction of the PKA had no significant effect on the number of defects.

Figure 8 shows the number of displaced atoms eventually produced inside the phase change material In, for which the PKA outgoing directions were ⟨001⟩, ⟨100⟩, ⟨110⟩, and ⟨135⟩. The values in each direction were the average of 10 simulated trajectories. The simulation analysis showed that the initial outgoing direction of the PKA had no effect on the final number of displaced atoms. After the PKA simulation in the four directions reached the equilibrium state, most of the displaced atoms were located at the normal lattice sites, and these atoms were replacement atoms. A small number of
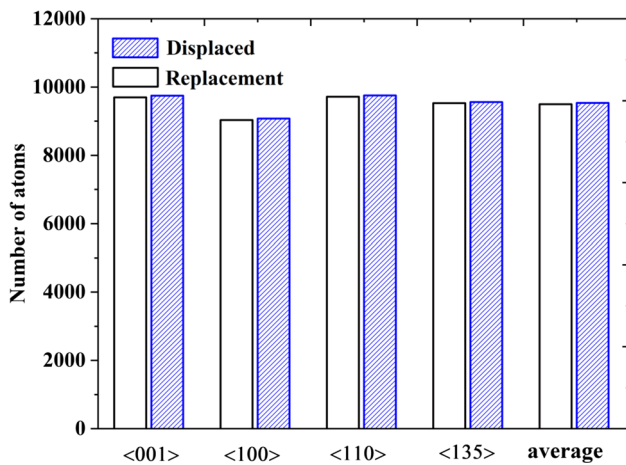
Fig. 8 Mean curves of the displaced atoms and displaced atoms in the four outgoing directions finally generated by PKA with 10 KeV kinetic energy in In

Fig. 9 Curve of the In fixed point phase change process, the phase change inflection point, and the selection of the supercooling point

atoms were located in interstitial sites to form the FP. For the four directions ⟨001⟩, ⟨100⟩, ⟨110⟩, and ⟨135⟩ of the PKA, 99.5%, 99.5%, 99.7%, and 99.7% of the displaced atoms were replacement atoms, respectively. This indicated that about 0.3% of the displaced atoms in the In formed defects, and about 99.7% of the displaced atoms migrated to lattice sites without forming defects.

After the cascade collision, the material entered the annealing stage, which lasted longer. At this stage, point defects formed by cascade collisions migrated and aggregated, forming clusters of defects such as Frank dislocation rings, voids, and stacking fault tetrahedrons. Related researchers have also studied the irradiation defect clusters in the steady-state stage. For example, in body-centered cubic iron, defects are mainly movable dislocation loops and C15 clusters[29]. In face-centered cubic copper, defects are mainly movable dislocation loops, immovable dislocation loops, and stacking fault tetrahedrons [30]. In hexagonal zirconium, defects are mainly movable basal dislocation loops and immovable cylindrical dislocation loops [31]. This large-scale evolution can better reflect the correlation between defects and material properties, but there are few studies on tetrahedral materials, which is also a future research direction.

4.2 Experimental analysis of phase change of irradiated samples

According to the theoretical simulation, after the spaceborne temperature standard carrying the In fixed point was affected by cosmic rays, the energy of the high-energy protons was mainly deposited on the fixed point material In, resulting in irradiation defects inside the In. However, the specific effect of this defect on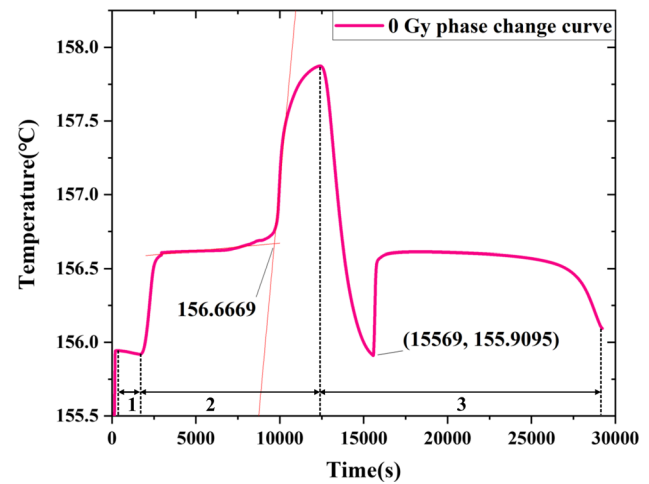 the phase change characteristics of the fixed point was unknown. Therefore, this section describes how the effects of proton irradiation on the undercooling, phase change plateau, phase change temperature, and melting time of the In fixed point were investigated with experiments on six different radiation doses of In phase change fixed point crucible samples.

Figure 9 shows the curves of the phase change process for one cycle of the In fixed point. For high purity In, the melting plateau was almost horizontal; so, the average value of the stable part of the melting plateau was taken as the melting temperature of the fixed point. Linear fitting was performed on the stable part of the melting plateau and the heating stage after the phase change; the intersection point was defined as the melting "inflection point", and the stable part was the melting plateau time. In this research, the "inflection point" was uniformly selected as the melting plateau value. For the freezing platform, due to the obvious supercooling phenomenon of the In, the freezing plateau time was defined from the highest point after the supercooling of the In fixed point to the cooling stage after the completion of the phase change. The average value of 50% of the data in the middle of the freezing plateau was taken as the freezing plateau value.

In this experiment, six irradiation doses (0 Gy, 99.5 Gy, 199 Gy, 298 Gy, 398 Gy, and 597 Gy) were selected for testing, and a total of six In phase change fixed point crucible samples were obtained, from No. 1 to No. 6. Four consecutive replicate experiments were performed on each sample to measure the phase change process. The measurement results are shown in Fig. 10. It was obvious that the irradiated sample was more stable than the unirradiated sample. The internal temperature of the irradiated In fixed point crucible increased, the molecular thermal motion ability was enhanced, and the fixed point material was evenly distributed; so, the plateau was more stable.
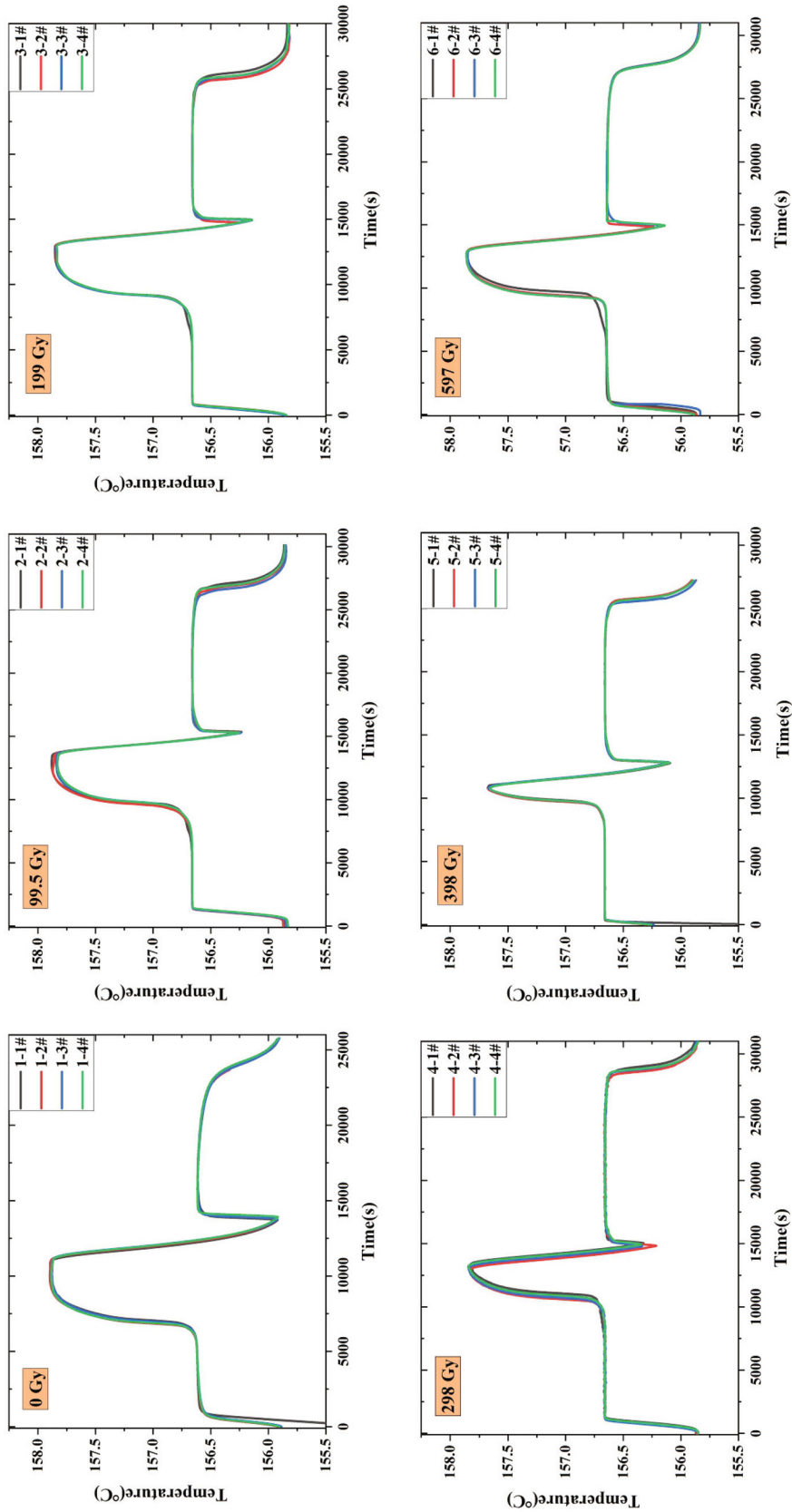
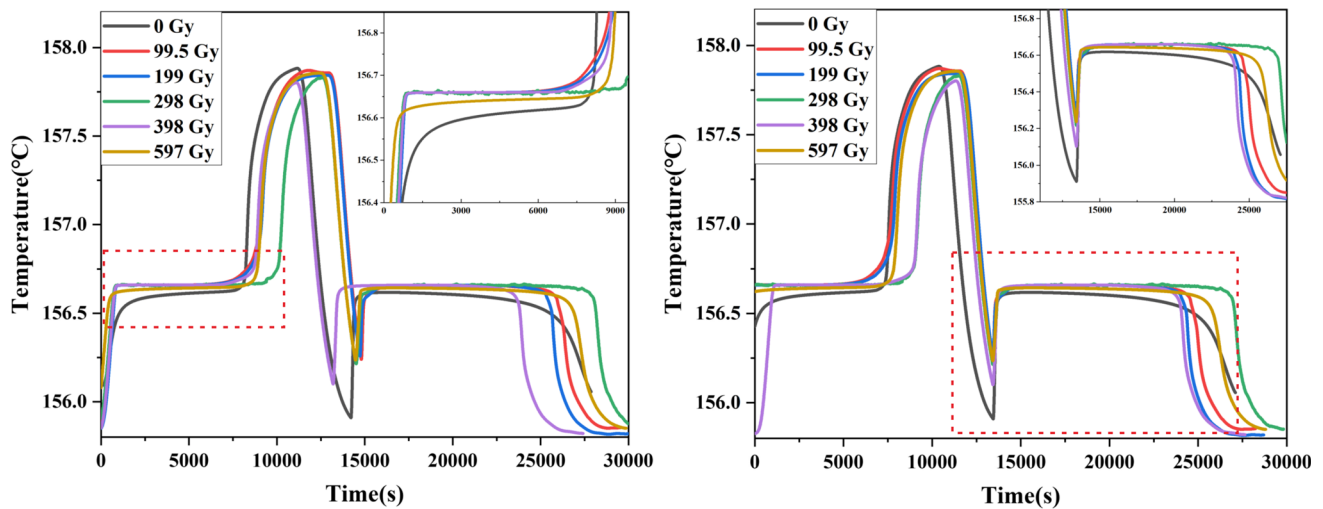**Fig. 10** Experimental results of four In phase change fixed point crucible samples

Fig. 11 Melting curves of samples with different irradiation doses and unirradiated samples

Table 2 Fixed point crucible experiment with different irradiation doses

Irradiation doses	Supercooling point/°C	Melting plateau value /°C	Melting time/min	Freezing plateau value/°C	Freezing time/min
1 (0 Gy)	155.9094	156.6314	61	156.6122	96
2 (99.5 Gy)	156.2389	156.6641	130	156.6588	125
3 (199 Gy)	156.2581	156.6642	130	156.6588	125
4 (298 Gy)	156.2144	156.6647	135	156.6582	164
5 (398 Gy)	156.1011	156.6612	130	156.6583	126
6 (597 Gy)	156.2346	156.6537	110	156.6383	155

Figure 11 shows the summary curve of the phase change experiments on six different irradiation dose samples and non-irradiated samples, and the experimental results are summarized in Table 2. The irradiated sample dose of Nos. 2-5 represents the irradiation dose of the spaceborne temperature sensor during the 15 years of orbital operation. Observing the phase change experiments of all samples, it can be seen that the phase change temperature value of the irradiated In fixed point was higher than that of the unirradiated In fixed point. The melting time was also significantly longer than that of the unirradiated samples, and this phenomenon did not change with the increasing melting times. By calculating the standard deviation of the melting plateau and the freezing plateau of the In fixed point on-orbit for 15 years, the stability values were obtained as 6 mK and 8 mK. The melting plateau value of In fixed point before and after irradiation show that the phase change temperature of In increases by about 30 mK after proton irradiation, and the phase transition temperature of In after proton irradiation increased by about 30 mK.

The theoretical simulation showed that vacancies were generated inside the In fixed point after proton irradiation, and the FP formed by these vacancies and interstitial atoms acted as an impurity of high-purity In, which indirectly affected the supercooling point value of the fixed point. It can be seen from the experimental data that the supercooling point of the In fixed point after irradiation increased and the supercooling degree decreased, that is, the freezing time of the In fixed point was shortened. Averaging the increments of the subcooling points of the irradiated samples revealed that the subcooling decreased by 0.3 °C after irradiation.

5 Conclusion

In this research, we investigated the effect of cosmic rays irradiation on the phase change characteristics of an In fixed point that could be applied to a spaceborne temperature sensor. The energy deposition and the distribution of high-energy protons at fixed points were simulated. The formation process of irradiation defects in the fixed point material In was demonstrated with molecular dynamics simulation. According to the simulation analysis, it was known that when a proton was irradiated onto the In fixed point crucible, the proton energy was mainly deposited on the In fixed point, which caused FP to be generated inside the In fixed point. The defect atoms had obvious recovery behavior. Therefore, after the PKA simulation reached the equilibrium state, about 0.3% of the displaced atoms migrated to the interstitial posi-

tion to form FP, and about 99.7% of the displaced atoms migrated to the lattice sites of the other atoms to form replacement atoms. Additionally, it was determined that the initial outgoing direction of the PKA did not affect the final number of defective atoms.

The experimental system was also set up to perform phase change experiments on six In phase change fixed point crucible samples with different radiation doses. The phase change temperature value of the irradiated In fixed point was 30 mK higher than that of the unirradiated In fixation point, the phase change time was significantly longer than that of the irradiated samples, and the phase change plateau was more stable. Since the FP generated by proton irradiation as an impurity indirectly affected the supercooling point value of the fixed point, the experimental results showed that the subcooling degree decreased by 0.3 °C after irradiation.

Data Availability Statement This manuscript has no associated data or the data will not be deposited. [Authors' comment: The datasets generated during and/or analysed during the current study are available from the corresponding author on reasonable request].

References

1. V.N. Krutikov et al., Metrologia **43**(2), 94 (2006)
2. F.A. Best et al., Proc. of SPIE. **9263**, 172–181 (2014)
3. L. Naineng et al., j. Remote. Sens (Chin.) **24**(6), 672–680 (2020)
4. P.T. Hugh et al., Metrologia **27**(1), 3–10 (1990)
5. R.H. Sima et al., Measurement **168**, 108462 (2021)
6. F.A. Best et al., Proc. SPIE. **8527**, 74–83 (2012)
7. R.H. Sima et al., IEEE. T. Geosci. Remot. Sens. **59**(7), 6266–6276 (2020)
8. X.P. Hao et al., Int. J. Thermophys. **38**(6), 1–13 (2017)
9. J. Widiatmo et al., Int. J. Thermophys. **38**(3), 1–14 (2017)
10. T..S.. Topham et al., NPJ Microgravity **1**(1), 1–5 (2015)
11. X.P. Hao et al., Metrologia **57**(6), 065016 (2020)
12. X.P. Hao et al., IEEE. T. Geosci. Remot. Sens. **60**, 1–8 (2022)
13. E. Wakai et al., J. Nucl. Mater. **543**, 152503 (2021)
14. Y. Katoh et al., J. Nucl. Mater. **417**(1–3), 416–420 (2011)
15. L. Snead et al., J. Nucl. Mater. **340**(2–3), 187–202 (2005)
16. D. Rapaport et al., Comput. Phys. **10**(5), 456–456 (1996)
17. E.C. Do et al., Calphad **32**(1), 82–88 (2008)
18. J.F. Ziegler, J.P. Biersack, Treatise on heavy-ion science, 93–129. Springer (1985)
19. S. Plimpton, J. Comput. Phys. **117**(1), 1–19 (1995)
20. J.F. Briesmeister et al., LA-13709-M, 2. Los Alamos National Laboratory (2000)
21. S.H. Yang et al., Phys. Rev. B **57**(4), 2013 (1998)
22. W.G. Hoover et al., Phys. Rev. A **31**(3), 1695 (1985)
23. W.G. Hoover et al., Phys. Rev. A **34**(3), 2499 (1986)
24. S. Melchionna et al., Mol. Phys. **78**(3), 533–544 (1993)
25. K. Nordlund et al., Phys. Rev. B **57**(13), 7556 (1998)
26. L. Van Brutzel et al., J. Nucl. Mater. **358**(2–3), 209–216 (2006)
27. X.F. Tian et al., Nucl. Instrum. Meth. B **269**(15), 1771–1776 (2011)
28. X.F. Tian et al., Nucl. Instrum. Meth. B **321**(5), 24–29 (2014)
29. A. Chartier et al., Acta Mater. **180**, 141–148 (2019)
30. D.J. Bacon et al., J. Nucl. Mater. **276**(1), 1–12 (2000)
31. C. Maxwell et al., J. Nucl. Mater. **531**, 151979 (2020)